ACCEPTED FOR PUBLICATION IN THE ASTROPHYSICAL JOURNAL
Preprint typeset using LaTeX style emulateapj v. 08/22/09

REVISED METALLICITY CLASSES FOR LOW-MASS STARS: DWARFS (DM), SUBDWARFS (SDM), EXTREME SUBDWARFS (ESDM), AND ULTRA SUBDWARFS (USDM).[1,2]

SÉBASTIEN LÉPINE[3], R. MICHAEL RICH[4], AND MICHAEL M. SHARA[3]

Accepted for publication in the Astrophysical Journal

ABSTRACT

The current classification system of M stars on the main sequence distinguishes three metallicity classes (dwarfs - dM, subdwarfs - sdM, and extreme subdwarfs - esdM). The spectroscopic definition of these classes is based on the relative strength of prominent CaH and TiO molecular absorption bands near 7000, as quantified by three spectroscopic indices (CaH2, CaH3, and TiO5). The boundaries between the metallicity classes were initially defined from a relatively small sample of only 79 metal-poor stars (subdwarfs and extreme subdwarfs). We re-examine this classification system in light of our ongoing spectroscopic survey of stars with proper motion $\mu > 0.45''$ yr^{-1}, which has increased the census of spectroscopically identified metal-poor M stars to over 400 objects. Kinematic separation of disk dwarfs and halo subdwarfs suggest deficiencies in the current classification system. Observations of common proper motion doubles indicates that the current dM/sdM and sdM/esdM boundaries in the [TiO5,CaH2+CaH3] index plane do not follow iso-metallicity contours, leaving some binaries inappropriately classified as dM+sdM or sdM+esdM. We propose a revision of the classification system based on an empirical calibration of the TiO/CaH ratio for stars of near solar metallicity. We introduce the parameter $\zeta_{TiO/CaH}$ which quantifies the weakening of the TiO bandstrength due to metallicity effect, with values ranging from $\zeta_{TiO/CaH} = 1$ for stars of near-solar metallicity to $\zeta_{TiO/CaH} \simeq 0$ for the most metal-poor (and TiO depleted) subdwarfs. We redefine the metallicity classes based on the value of the parameter $\zeta_{TiO/CaH}$; and refine the scheme by introducing an additional class of ultra subdwarfs (usdM). We introduce sequences of sdM, esdM, and usdM stars to be used as formal classification standards.

Subject headings: stars: abundances — stars: fundamental parameters — stars: low-mass, brown dwarfs — stars: Population II — stars: subdwarfs — Galaxy: solar neighborhood

1. INTRODUCTION

Stars known as *red dwarfs* and *red subdwarfs*, are main sequence stars of spectral type M, typically meant to include all main sequence objects of spectral subtype K5 to M9. These cool, low-mass stars are the most abundant stars in the Galaxy. They are ubiquitous in the vicinity of the Sun, where they are readily identified as faint stars with large proper motions. These stars also have tremendous potential as tracers of the chemical and dynamical evolution of the Galaxy, not only because of the sheer number of them, but also because their lifetimes are much greater that the Hubble time (Laughlin, Bodenheimer, & Adams 1997), and because metallicity variations have dramatic effects on their spectral energy distribution. The optical and near infrared spectra of M dwarfs and subdwarfs are dominated by molecular absorption bands of metal oxides and hydrides, most prominently bands of TiO and CaH (Bessel 1991). The ratio between the strength of the oxide and hydride bands has long been known as a metallicity diagnostic (Bessel 1982). The high-velocity red subdwarfs, kinematically associated with the Galactic halo, consistently display shallower TiO absorption bands than the more common red dwarfs associated with the Galactic disk. Atmospheric models show that metallicity variations in cool and ultra-cool stars have dramatic effects on their optical spectra (Allard & Hauschildt 1995). This is useful because low-resolution spectroscopy is sufficient for measuring both effective temperature and metallicity effects.

The current classification system of cool (spectral subtypes K5-M6) and ultra-cool (subtypes M7-M9) low-mass stars distinguishes three broad metallicity classes: the dwarfs (K5-M9, or dK5-dM9), the metal-poor subdwarfs (sdK5-sdM9), and the very metal-poor extreme subdwarfs (esdK5-esdM9). Dwarf (dM) stars are generally associated with the Galactic disk population and show strong bands of both TiO and CaH. Spectral subtypes from K5 to M9 are assigned based on a sequence of standard objects (Kirkpatrick, Henry, & McCarthy 1991). The key feature is the strength of the optical TiO bands, with VO bands also used to discriminate the M7-M9 "ultra-cool" subtypes (Kirkpatrick, Henry, & Simons 1995). Spectral subtypes of K and M dwarfs have also been calibrated relative to spectral indices measuring the strengths of various molecular bandheads. The most popular set of indices was defined by Reid, Hawley, & Gizis (1995), and expanded by Lépine, Rich, & Shara (2003a). These spectral indices are useful in directly deriving spectral subtypes from simple spectroscopic measurements.

The metal-poor subdwarfs (sdM) and extreme subdwarfs (esdM) are for the most part kinematically associated with the Galactic halo, and display relatively weaker bands of TiO while retaining strong CaH absorption (Hartwick, Cowley, & Mould 1984; Ruiz & Anguita 1993; Gizis 1997; Gizis & Reid 1997; Lépine, Rich, & Shara 2003a; Scholz *et al.* 2004a; Phan-Bao & Bessel 2006). A classification system for subdwarfs was introduced by Gizis

[1] Based on observations conducted at the MDM observatory, operated jointly by the University of Michigan, Dartmouth College, the Ohio State University, Columbia University, and the University of Ohio.

[2] Based on observations conducted at the Lick Observatory, operated by the University of California system.

[3] Department of Astrophysics, Division of Physical Sciences, American Museum of Natural History, Central Park West at 79th Street, New York, NY 10024, USA, lepine@amnh.org, mshara@amnh.org

[4] Department of Astrophysics, University of California at Los Angeles, Los Angeles, CA 90095, USA, rmr@astro.ucla.edu

TABLE 1
SPECTRAL INDICES FOR LOW-MASS SUBDWARFS[a]

Index Name	Numerator(Å)	Denominator(Å)
CaH2	6814-6846	7042-7046
CaH3	6960-6990	7042-7046
TiO5	7126-7135	7042-7046

[a] Indices originally defined by Reid, Hawley, & Gizis (1995); the indices are calculated from the ratio of the *average flux* over the specified wavelength ranges.

(1997, hereafter G97), and is based on measurements of the four spectroscopic indices (CaH1, CaH2, CaH3, and TiO5) defined by Reid, Hawley, & Gizis (1995). These indices measure the strength of the main CaH and TiO bands located near 7,000Å. Separation into the three metallicity classes is determined by the relative strengths of the CaH1, CaH2, and CaH3 spectral indices relative to the TiO5 spectral index, using arbitrarily defined relationships. Subtypes are assigned based on the combined strengths of the CaH2 and CaH3 indices. The system was initially defined for earlier subtypes, down to ∼sdM5/esdM5, but has since been extrapolated to cooler subtypes (Schweitzer *et al.* 1999; Lépine, Shara, & Rich 2003, 2004; Scholz, Lodieu, & McCaughrean 2004), and subdwarfs are now being identified well into the L type regime (Lépine, Rich, & Shara 2003b; Burgasser *et al.* 2003; Gizis & Harvin 2006).

In the G97 system the separation between dwarfs, subdwarfs, and extreme subdwarfs is determined using a combinations of four relationships defined in [CaH1,TiO5], [CaH2,TiO5], and [CaH3,TiO5]. Following Lépine, Shara, & Rich (2003), it has however become customary to represent the spectroscopically confirmed subdwarfs in a single diagram of CaH2+CaH3 versus TiO5 (Lépine, Shara, & Rich 2004; Scholz *et al.* 2004a; Reid & Gizis 2005). A simplification of the G97 system was thus proposed by Burgasser & Kirkpatrick (2006), using only two relationships defining dM/sdM/esdM separators in the [CaH2+CaH3,TiO5] diagram. The separators were validated using previously classified objects, and are thus essentially equivalent to the original G97 system.

In this paper, we re-examine the classification system for red dwarfs and subdwarfs in light of new spectroscopic measurements of 1,983 high proper motion stars from the LSPM-north proper motion catalog (Lépine & Shara 2005). We redefine the metallicity subclasses based on a calibration of the TiO to CaH ratio for stars of Solar metallicity. We introduce the $\zeta_{TiO/CaH}$ metallicity index, which we demonstrate to be an simple and objective measurement of the metal content in M dwarfs and subdwarfs. The index therefore provides an objective criterion to redefine the metallicity subclasses. We propose an update of the classification system which uses four metallicity subclasses instead of the previous three, introducing the new subclass of "ultra subdwarfs" (usdK, usdM) which includes stars with the lowest apparent metal content. We introduce new spectroscopic sequences of subdwarfs, extreme subdwarfs, and ultra subdwarfs, which can be used as classification standards.

2. CURRENT CENSUS OF SPECTROSCOPICALLY CONFIRMED M SUBDWARFS

2.1. *Previously classified objects*

The system currently in use to classify the M subdwarfs is based on the strength of the TiO and CaH molecular bands near 7000Å, as quantified by the three spectral indices CaH2, CaH3, and TiO5, defined by Reid, Hawley, & Gizis (1995). The CaH2 and CaH3 indices measure the mean flux level in parts of the main CaH band, as measured relative to the mean flux in a reference point set at 7044Å(which defines a local pseudo continuum). The TiO5 index measures the mean flux level in a region within the nearby TiO band, as measured relative to the same pseudo-continuum reference point. The formal index definitions are recopied in Table 1. The location of all the reference points is illustrated in Figure 1 of Reid, Hawley, & Gizis (1995) and in Figure 1 of Lépine, Shara, & Rich (2003). The indices are defined in such a way that they yield a value of 1 if the band is undetected (i.e. the depth of the bandhead is at the continuum level), and 0 if the band is completely saturated.

We have searched the literature for spectroscopically confirmed M dwarfs and subdwarfs, for which values of the CaH2, CaH3 and TiO5 indices have been measured and recorded. These include most of the stars classified as M dwarfs in the Solar Neighborhood ($d < 25$pc), and all the spectroscopically confirmed M subdwarfs. The distribution in the [CaH2+CaH3,TiO5] diagram is shown in Figure 1 (filled triangles, open circles).

Historically the first set of objects for which values of CaH2, CaH3 and TiO5 were recorded are the 1,971 nearby dwarfs from the Palomar-MSU spectroscopic survey (Reid, Hawley, & Gizis 1995). High proper motion stars from W. J. Luyten's *LHS catalog* were then targeted: 71 K and M dwarfs were classified by Gizis & Reid (1997), then 79 K and M subdwarfs were classified by Gizis (1997). These stars were the fundamental sample from which Gizis (1997) established the M subdwarf classification system based on the molecular band indices. Stars from this initial sample are noted with filled triangle symbols in Fig.1. The census of spectroscopically confirmed M subdwarfs and extreme M subdwarfs was then relatively small, and many additions have been made since then.

Most of the new additions came from follow-up spectroscopy of faint stars with large proper motions, including objects listed in the *LHS catalog*, and newly discovered stars from the SuperCosmos sky survey (Hambly *et al.* 2001), the Liverpool-Edinburgh proper motion survey (Pokorny *et al.* 2003), and the SUPERBLINK proper motion survey (Lépine & Shara 2005). Some of the newest additions have been pushing the limits of the classification system to ever cooler subdwarfs. The latest objects in the G97 system were LHS 377, an sdM7.0 subdwarf, and LHS 1742a, an esdM5.5 extreme subdwarf; much later stars have been identified since. The high proper motion star APMPM J0559-2903 was classified an esdM7.0 by Schweitzer *et al.* (1999), while LSR 1425+7102 was classified an sdM8.0 (Lépine, Shara, & Rich 2003). The very high proper motion object LSR 1610-0040 was initially classified as an sdL by Lépine, Rich, & Shara (2003b), though the star is now considered to be a moderately metal-poor late-M dwarf/subdwarf (Cushing & Vacca 2006). Scholz *et al.* (2004a) identified three more very cool subdwarfs, including SSSPM J1013-1356, classified as sdM9.5. Lodieu *et al.* (2005) classified the new high proper motion star SSSPM J0500-5406 an esdM6.5, though values of the CaH2, CaH3 and TiO5 indices were not included in the paper. They were, however, provided

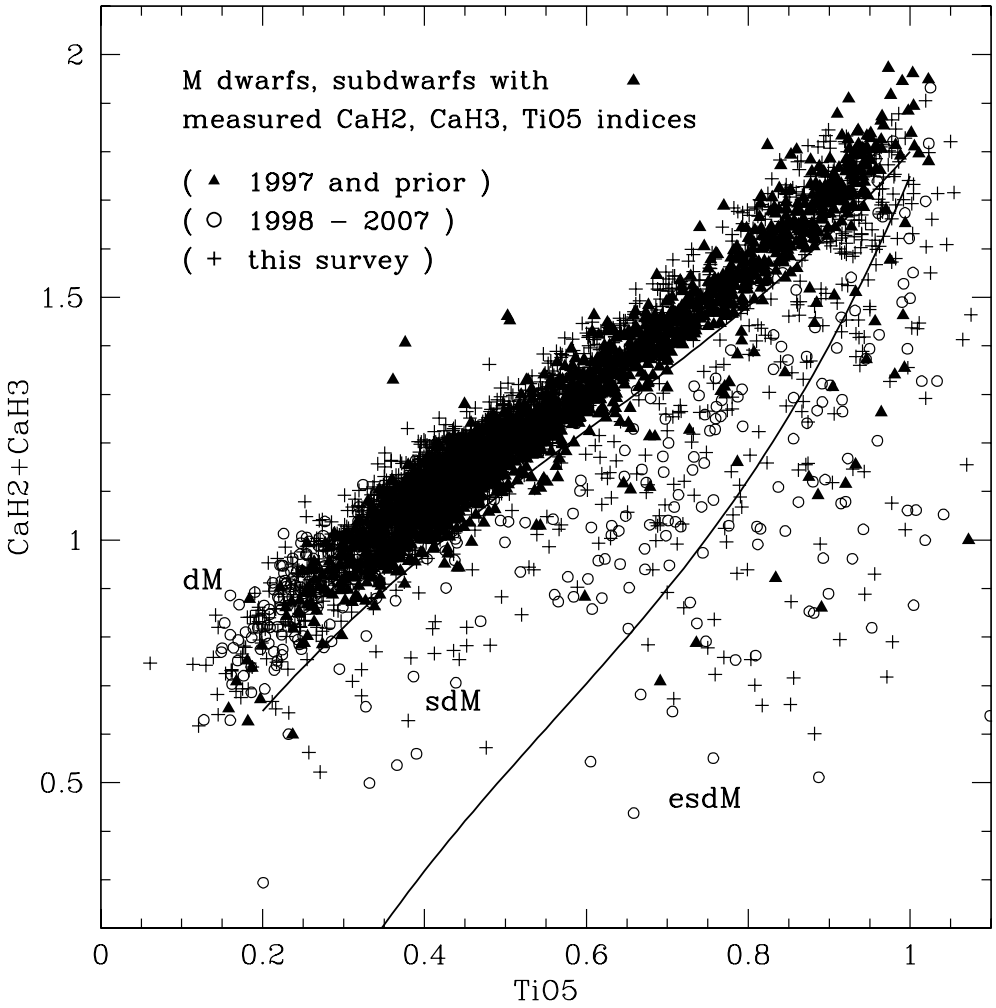

FIG. 1.— Top: distribution of spectroscopically confirmed, cool dwarfs and subdwarfs in the [CaH2+CaH3,TiO5] spectral indices diagram. Stars with spectral indices measured up until 1997 are marked as filled triangles. Stars identified from 1998 to 2007 are marked as open circles. Objects classified in our current, spectroscopic follow-up survey of high proper motion stars from the LSPM-north catalog are denoted by crosses. The two continuous lines marks the dM/sdM and sdM/esdM subclass separators, as proposed by Burgasser & Kirkpatrick (2006), which delimit the metallicity subclasses according to the system introduced by Gizis (1997).

by Burgasser & Kirkpatrick (2006), who re-observed SSSPM J0500-5406 and identified two more ultra-cool subdwarfs including LEHPM 2-59, classified as esdM8.0. The $3.5''$ yr^{-1} proper motion star SSSPM J1444-2019 was classified as an sdM9 (Scholz, Lodieu, & McCaughrean 2004). In all these cases, the spectral subtypes were determined by extrapolating the relationships defined by G97, in which the spectral subtype is a monotonic function of the CaH2 and CaH3 indices. Other late-type subdwarfs reported in the literature include the high proper motion star APMPM J1523-0245, classified as sdM5.5 (Gizis 1997), and a few late-M and L subdwarfs identified within the 2MASS survey (Burgasser *et al.* 2003, 2004; Burgasser 2004).

More extensive lists of new classifications included 257 dwarfs and subdwarfs from the *LHS catalog* Reid & Gizis (2005), and 104 M/sdM/esdM stars from the SUPERBLINK survey (Lépine, Rich, & Shara 2003a). All additions to the census of spectroscopically confirmed M dwarfs and subdwarfs made between 1998 and 2007 are displayed as open circles in Fig.1. The figure also shows the new dM/sdM and sdM/esdM separators as defined by Burgasser & Kirkpatrick (2006). The diagram demonstrates the relative scarcity of subdwarfs and extreme subdwarfs in the Solar Neighborhood, which are outnumbered by the dwarfs by two orders of magnitude.

2.2. *New spectroscopic survey*

We have been conducting a massive spectroscopic follow-up survey of sources from the LSPM-north catalog of stars with proper motions $\mu > 0.15''$ yr^{-1} (Lépine & Shara 2005). About half the stars in the LSPM-north catalog are re-identifications of stars from the Luyten catalogs, the other half are new discoveries, and the LSPM-north is thus an excellent source of new nearby M dwarfs and subdwarfs. Medium-resolution spectra with $\Delta\lambda \sim 1.7-2.3$ pixel^{-1} have been collected from the 2.4-meter Hiltner telescope at the MDM Observatory, the 3-meter Shane Telescope at the Lick Observatory, and the 4-meter Mayall Telescope on Kitt Peak. Our current target list includes all 2,966 stars from the LSPM-north which have proper motions $\mu > 0.45''$ yr^{-1}, with a priority to stars with no published spectroscopic data. Detailed results from the ongoing survey will be published in an upcom-

ing spectroscopic catalog (Lépine et al., *in preparation*). To this date, we have identified 1,983 stars in our survey which clearly display the broad, molecular absorption bands characteristic of low-mass, main sequence stars with spectral subtypes from K5 to M9, including significant numbers of subdwarfs and extreme subdwarfs.

We have been recording values of the CaH2, CaH3, and TiO5 indices for all the stars. With spectra of resolution 1.5Å-2.3Åper pixel, and signal-to-noise S/N$\sim$ 20, our index measurements have a typical accuracy of ≈ 0.03. A significant fraction of the stars, especially the subdwarfs, are found to have large radial velocities (consistent with Galactic halo membership); all spectra are thus red- or blue-shifted to their local rest frame before the spectroscopic indices are measured.

Our sample of newly classified dwarfs and subdwarfs spans a wide variety of relative and absolute CaH and TiO bandstrengths, which indicates that the sample covers a wide range of both effective temperatures and metal abundances. The newly classified stars are plotted in Fig.1 as crosses. The new sample fills up many holes left in the [CaH2+CaH3,TiO5] diagram by the previous census. Our follow-up survey thus represents a major addition to the list of spectroscopically confirmed M subdwarfs, and provides a much expanded sample of stars with recorded values of the CaH2, CaH3 and TiO5 indices.

The number of spectroscopically confirmed subdwarfs keeps increasing at a rapid pace. We expect current and planned surveys to significantly increase the number of spectroscopically confirmed subdwarfs. With a large dataset in hand, a re-evaluation of the classification system is now in order.

3. REVISITING THE METALLICITY SUBCLASSES OF LOW-MASS STARS

3.1. *Dwarf/subdwarf separation in the reduced proper motion diagram*

It has long been known that the high-velocity subdwarfs in the Solar vicinity, i.e. local stars from Population II, can be separated out from Galactic disk (Population I) stars using a reduced proper motion diagram (e.g. Jones 1971). A plot of the reduced proper motion against an optical-to-infrared color is known to provide a relatively clean separation between M dwarfs from the local disk population and M subdwarfs from the Galactic halo (Salim & Gould 2002). It is thus possible to isolate samples of Pop I dwarfs and Pop II subdwarf using reduced proper motion diagrams. Those samples can then be used to determine the expected distribution of metal-rich and metal-poor stars in the [CaH2+CaH3,TiO5] diagram, and objectively determine the boundary separating the M dwarfs and M subdwarfs.

We build a reduced proper motion diagram using the reduced proper motion in V magnitude $H_V = V + 5\log\mu + 5$ and the optical-to-infrared color V-J. The diagram is shown in Figure 2, and displays all the dwarfs and subdwarfs for which we could recover proper motions (μ), V magnitudes, and V-J colors. As expected, the stars fall in two fairly distinct loci, which correspond to the metal-rich disk and metal-poor halo stars, respectively. As is well-known, halo subdwarfs are separated from the disk M dwarfs both because of their relatively bluer color at a given absolute magnitude (Monet *et al.* 1992), and because of their larger mean transverse velocities. Both effects combine to move the M subdwarfs down and to the left of the main stellar locus.

We define two regions, denoted "Disk" and "Halo" which, based on the argument above, should contain a majority of metal-rich/disk stars and metal-poor/halo stars, respectively. One can show that the reduced proper motion $H_V = M_V + 5\log v_T - 3.38$, where M_V is the absolute magnitude in V and v_T is the projected velocity in the plane of the sky, in km s^{-1}. We assume the absolute magnitudes M_V to follow the color-magnitude relationship M_V=$M_V(V-J)$ of Lépine (2005), which was calibrated using a large sample of nearby dwarfs with accurate parallax measurements. The "Disk" region is hence defined in the [H_V,$V-J$] plane to includes all dwarfs with transverse velocities 5 km s^{-1} $< v_T <$ 100 km s^{-1}. Stars which fall below the "Disk" box in Fig.2 are thus either dwarfs with transverse velocities $v_T >$ 100 km s^{-1}, or stars which fall significantly below the M_V=$M_V(V-J)$ color-magnitude relationship for nearby disk dwarfs, e.g. subdwarf stars. The "Halo" region, on the other hand, selects for stars which are unambiguously high-velocity, Pop II stars. The upper boundary in Fig.2 selects for cool subdwarfs with transverse velocities $\gtrsim$ 150 km s^{-1}. The many stars which fall in the no man's land between the "Disk" and "Halo" regions probably include moderately metal-poor subdwarfs, or metal-rich stars with large transverse velocities. Such stars are likely to be associated with the Galactic thick disk.

Figure 3 shows separate [CaH2+CaH3,TiO5] diagrams for stars which fall into either the "Disk" or "Halo" selection boxes. Stars from the "Disk" group show a tight correlation between the CaH2+CaH3 and TiO5 indices (Fig.3, left panels). In contrast, stars from the "Halo" group display a wide variety of TiO bandstrengths for a given depth of the CaH bands. The "Halo" stars also have systematically smaller ratios of TiO to CaH, compared with the stars from the "Disk" group. This confirms our earlier impression that the kinematically selected "Disk" objects are indeed dwarf stars all of roughly solar metallicity, while the "Halo" objects are overwhelmingly metal-poor subdwarfs.

Assuming this scheme to be correct, then the two groups can be used as fiducial samples to more precisely determine the loci of dwarfs and subdwarfs in the [CaH2+CaH3,TiO5] diagram. This is especially useful to redefine the separator between the dwarf (M) and subdwarf (sdM) classes. A close examination of the top panels in Fig.3 shows that the current M/sdM separator is fairly conservative in assigning stars to the subdwarf (sdM) class. The vast majority of the "disk" stars (top left panel) are allocated to the dwarf (dM) class, with room to spare. Many stars from the "Halo" group, on the other hand, are not assigned to the subdwarf (sdM) class, as they most probably should be. This is especially apparent at earlier subtypes, i.e. for larger values of CaH2+CaH3 (top right of the diagram). This justifies at least a readjustment of the metallicity class separators proposed by Burgasser & Kirkpatrick (2006).

3.2. *The metallicity index* $\zeta_{\rm TiO/CaH}$

The kinematical selection of local disk dwarfs from the reduced proper motion diagram allows us to calibrate the ratio of TiO to CaH for stars of the disk, which contains stars of roughly solar metallicity. We use all the stars from the "disk" group, and obtain a fit of the TiO5 spectral index as a function of the CaH2+CaH3 index, yielding:

$$[\mathrm{TiO5}]_{Z_\odot} = -0.164(\mathrm{CaH2}+\mathrm{CaH3})^3 + 0.670(\mathrm{CaH2}+\mathrm{CaH3})^2 - 0.118(\mathrm{CaH2}+\mathrm{CaH3}) - 0.050 \quad (1)$$

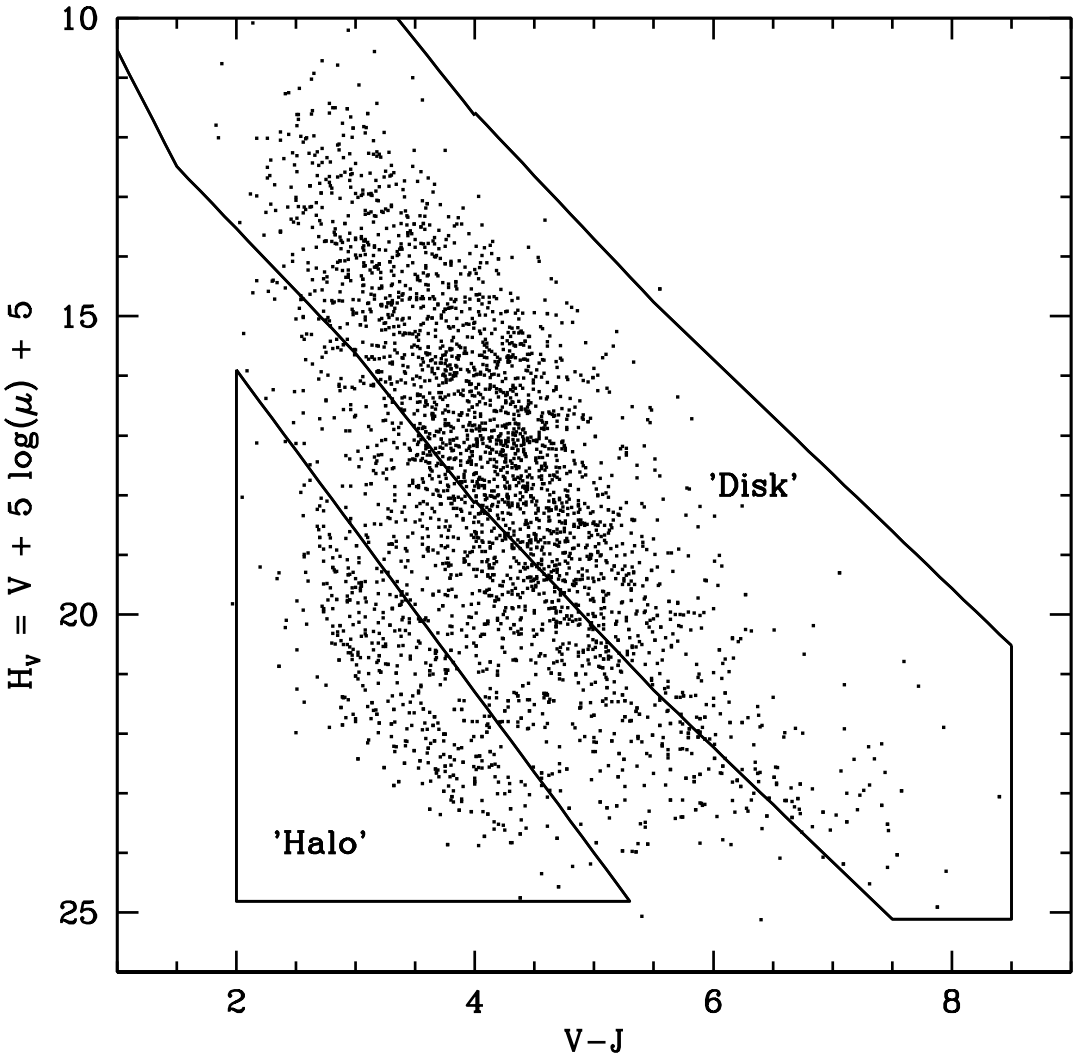

FIG. 2.— Reduced proper motion diagram of the M dwarfs and subdwarfs with formal spectral classification (see Fig.1). We identify two distinct groups: the "disk" stars, with generally low transverse velocities and standard color-magnitude relationship, and the "halo" stars with generally large transverse velocities and fainter magnitudes at a given color.

Equation 1 effectively provides a calibration of the TiO bandstrength relative to the CaH bandstrength, for stars of roughly solar metallicity ($Z_\odot$). This defines an objective reference point from which to estimate atmospheric abundances in subdwarfs spectra. While the depth of the CaH bands is used to estimate the effective temperature, the ratio of TiO to CaH is used to estimate the metallicity. A curve denoting $[TiO5]_{Z_\odot}$ as a function of CaH2+CaH3 is drawn in Fig.3 (dashed line). The "disk" stars are found tightly clustered along this curve, while the "halo" stars span a large range of TiO5 values with $[TiO5]_{Z_\odot} \lesssim TiO5 \lesssim 1.0$.

The relative strength of TiO to CaH in any one star can then be expressed relative to the (calibrated) strength of the TiO band in stars of solar metallicity using the parameter $\zeta_{TiO/CaH}$, which we define as:

$$\zeta_{TiO/CaH} = \frac{1 - TiO5}{1 - [TiO5]_{Z_\odot}}, \qquad (2)$$

where $[TiO5]_{Z_\odot}$ is given by Eq.1, and is a function of the CaH2+CaH3 index. The parameter $\zeta_{TiO/CaH}$ can thus be calculated for any star from its CaH2, CaH3, and TiO5 indices. All stars with abundances equal to the average abundance of stars in the Galactic disk will have $\zeta_{TiO/CaH}$ = 1, by definition. Metal-poor stars will have $\zeta_{TiO/CaH} < 1$, while stars with metal abundances larger than the Galactic disk average will have $\zeta_{TiO/CaH} > 1$.

Figure 4 displays a sequence of objects with similar CaH bandstrengths, but spanning a wide range of TiO bandstrengths, as determined by the CaH2+CaH3 and TiO5 spectral indices. Values of $\zeta_{TiO/CaH}$ are noted for each star, along with spectral subtypes. The stars clearly follow the expected trends, with the extreme subdwarfs (esdM) having the smallest values of $\zeta_{TiO/CaH}$, and the M dwarfs the largest. The spectra in Fig. 4 therefore trace metallicity effects in M dwarfs and subdwarfs.

We can test the consistency of $\zeta_{TiO/CaH}$ as a metallicity index by comparing the values of $\zeta_{TiO/CaH}$ measured in the components of resolved binary systems, where the two stars are

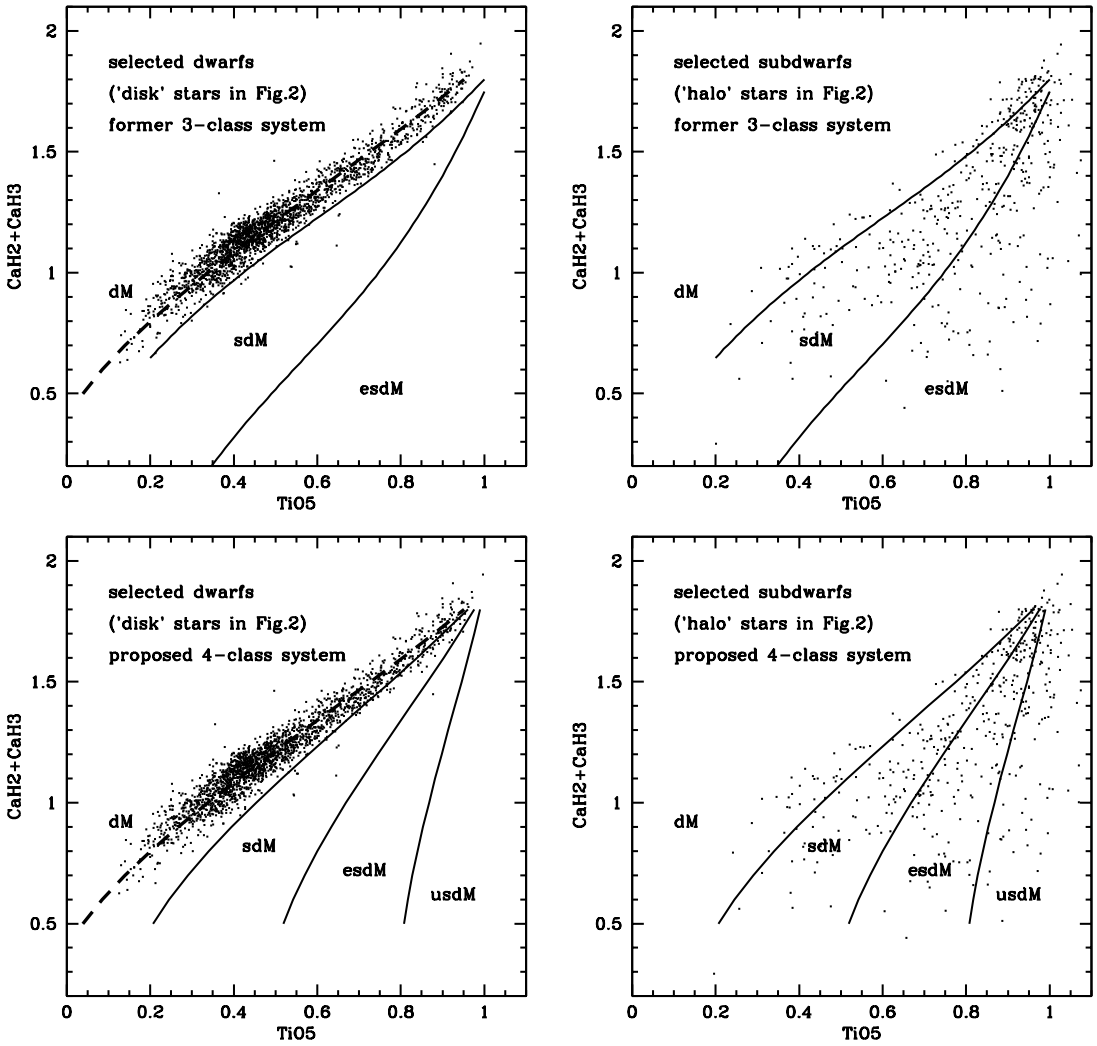

FIG. 3.— Top left: Comparison between the CaH and TiO bandstrengths of the stars in the "Disk" group, as defined in Fig.2. The TiO and CaH bandstrengths are tightly correlated, which indicates that the stars have equivalent (Solar) metallicities. Top right: CaH and TiO bandstrength for stars in the "Halo" group (see Fig.2). The TiO bands are systematically weaker than those of the "Disk" groups, which confirms that they are indeed drawn from a metal-poor population (Pop II). Stars are also found with a broad range of TiO/CaH ratios, which indicates that they span a wide range of metal abundances. Bottom left: new separators for the proposed 4-class system, which are based on the calibration of the CaH2+CaH3/TiO5 relationship for disk dwarfs (dashed line). Bottom right: distribution of the "Halo" stars in the 4-class system.

expected to share the same abundance. Our catalog contains 71 pairs of common proper motion doubles in which both components are in the K5-M9 subtype range. Two of the pairs are subdwarfs, four are extreme subdwarfs, all others are dwarfs. We compare the values of $\zeta_{TiO/CaH}$ for the primaries and secondaries in Figure 5. Values of $\zeta_{TiO/CaH}$ for the primaries and secondaries are found to be tightly correlated. This is possible if and only if (1) the components of high proper motion pairs share the same metallicity, and (2) the parameter $\zeta_{TiO/CaH}$ is a consistent measure of the metallicity in low-mass stars of different masses. This suggests a use for the parameter $\zeta_{TiO/CaH}$ in refining the metallicity subclass system in low-mass stars, and redefining the subclass separators in the CaH2+CaH3/TiO5 diagram.

3.3. *New metallicity classes: dwarfs, subdwarfs, extreme subdwarfs, and ultra subdwarfs*

As demonstrated above, the parameter $\zeta_{TiO/CaH}$ can be used as a simple yet objective estimate of the metal content in cool stars. We therefore use it to redefine the traditional metallicity subclasses (dwarf, subdwarf, extreme subdwarf) of low-mass stars. The fact that the parameter is based on the widely used CaH2 and CaH3 spectral indices allows for a direct comparison with earlier work, and the reclassification of previously observed objects using data already available in the literature.

Ideally, one would want a new definition which preserves as much as possible any previous subclass assignment. Unfortunately, the class separators defined by Burgasser & Kirkpatrick (2006) do not strictly run along lines of constant $\zeta_{TiO/CaH}$ (see below). Hence if we define a new sdM/esdM subclass separator that mostly agrees with the old separator at *earlier* subtypes (e.g. near CaH2+CaH3$\simeq$ 1.5), then most of the stars would fall into the sdM subclass, with only a few left in the esdM subclass. Such a separation would

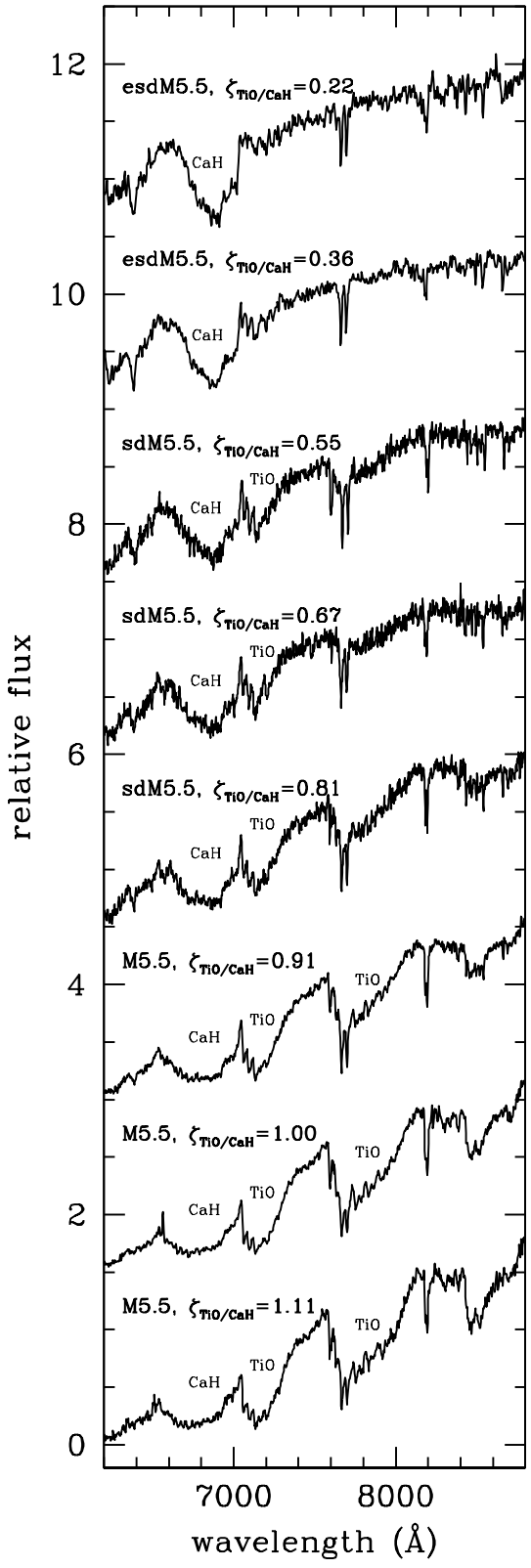

FIG. 4.— Effects of metallicity on the spectra of cool dwarfs and subdwarfs. These low-mass stars of similar [CaH2+CaH3] index values are shown in order of increasing $\zeta_{TiO/CaH}$, from top to bottom. The metal abundance is reflected in the relative strength of the TiO bandhead to the CaH bandhead. Spectral subtypes are noted, as well as values of the $\zeta_{TiO/CaH}$ index which quantifies the ratio between the TiO and CaH bandstrengths and is thus a marker for metallicity effects.

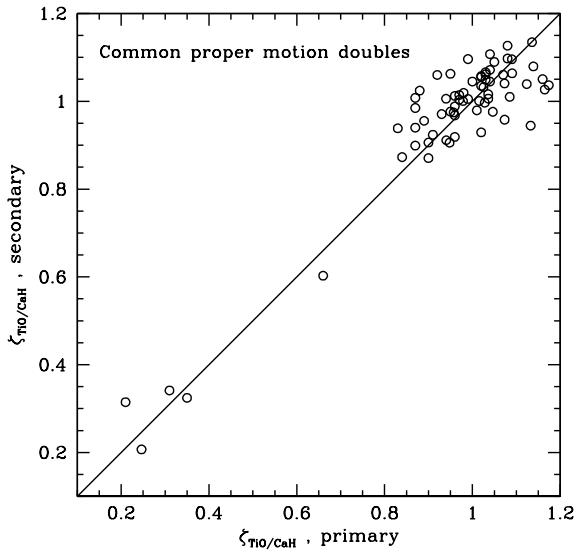

FIG. 5.— Comparison between the $\zeta_{TiO/CaH}$ metallicity index in the resolved primaries and secondaries of 71 common proper motion doubles. The tight correlation suggests that $\zeta_{TiO/CaH}$ is a good measure of relative metallicity in cool stars of various spectral subtypes.

not be very useful for the sample at hand. If on the other hand, we define a new sdM/esdM separator that matches the old one at *later* subtypes (e.g. near CaH2+CaH3$\simeq$ 0.5), then the new separator would put a majority of stars in the esdM class. This would fail to set up any distinction for the most extreme metal-poor stars in the sample.

Our solution to this dilemma is (1) to have the new sdM/esdM separator fall near the old separator at *later* subtypes and (2) to introduce a fourth class of objects which would regroup the most extreme of the subdwarfs, by the weakness of their TiO bandstrength. We propose to designate stars from the new, fourth category as "ultra subdwarfs". We find that the introduction of a fourth subclass gives additional depth to the system and highlights the subdwarfs with the most extreme properties, which strongly stand out in the [CaH2+CaH3,TiO5] diagram. We denote stars from the ultra-subdwarf class as "usdK" or "usdM".

The new four metallicity subclasses for low-mass stars are formally defined using our $\zeta_{TiO/CaH}$ metallicity index following:

$$\begin{aligned} \zeta_{TiO/CaH} &> 0.825 \Rightarrow \mathrm{K-M} \\ 0.500 < \zeta_{TiO/CaH} &< 0.825 \Rightarrow \mathrm{sdK-sdM} \\ 0.200 < \zeta_{TiO/CaH} &< 0.500 \Rightarrow \mathrm{esdK-esdM} \\ \zeta_{TiO/CaH} &< 0.200 \Rightarrow \mathrm{usdK-usdM} \end{aligned}$$

These separators are drawn in Fig.3 (upper right and lower right panels). Note that this new formal definition, based on ranges of the $\zeta_{TiO/CaH}$ parameter, retains some flexibility in that it allows for possible future refinements in the calibration of $[TiO5]_{Z_\odot}$.

We have already shown in Fig.5 that values of the parameter $\zeta_{TiO/CaH}$ are tightly correlated for components of common proper motion pairs. In Figure 6, we use the double stars again to demonstrate the consistency of the new 4-subclass system. The pairs are represented in the [CaH2+CaH3,TiO5] diagram. Individual components are plotted with star symbols, with line segments joining the components of each pair.

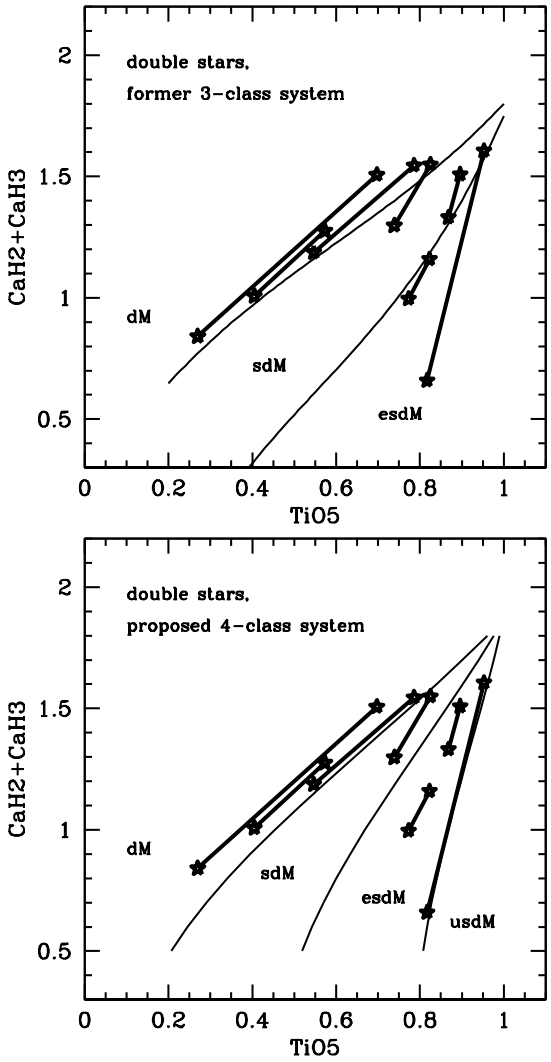

FIG. 6.— Distribution of TiO5 and CaH2+CaH3 index values for members of common proper motion pairs. The primaries and secondaries are connected by straight lines. In the former classification system, some pairs straddle the subclass separators, and have the secondary assigned to a different metallicity subclass than the primary. The new system more consistently assigns primaries and secondaries to the same metallicity class, which is what one should expect assuming that components in a pair should have similar abundances.

The subclass separators from both the old three-class and new four-class systems are drawn for comparison.

It is quite apparent from this plot that the new system provides a more satisfactory separation between the metallicity groups. In the old system, the segments joining the components clearly do not run parallel to the subclass separators. One of the pairs straddles the dM/sdM boundary, with the primary classified as a dwarf and the secondary and sdM. Another pair has an sdM primary, with a secondary located deep within the esdM zone. This runs afoul of the assumption that both components of wide binaries should have similar abundances. In the new system, however, the separators run nearly parallel to the double star segments. The most metal-poor of pair actually has both the primary and secondary sitting on the esdM/usdM separator, which is precisely what one would expect of the subclass separators, i.e. that they follow lines of iso-metallicity in the [CaH2+CaH3,TiO5] plane.

An additional check to the dwarf/subdwarf separator consists of placing all classified objects back in the reduced proper motion diagram. We do this in Figure 7, where we plot the stars from each metallicity subclass in a different symbol/color. One recovers the striking separation between the dwarfs and subdwarfs, which associates the dwarfs with the Galactic disk, and the subdwarfs with the Galactic halo (see Fig.2). The subdwarfs, extreme subdwarfs, and ultra subdwarfs also show some level of segregation in the reduced proper motion diagram. The ultra subdwarfs cluster in the extreme lower left of the diagram, with the extreme subdwarfs and subdwarfs roughly falling in successive layers above and to the right. This is consistent with the idea of a dependence of the color-magnitude relationship on metallicity. It could also indicate that the more metal-poor stars tend to have larger transverse velocities, and hence large reduced proper motions. Possibly, both kinematics and metallicity effects conspire to yield the slightly different observed loci for the subdwarfs, extreme subdwarfs, and ultra subdwarfs.

One limitation of the classification system become apparent in Fig.7, however. At the earliest subtypes, i.e. for stars with CaH2+CaH3$\gtrsim$1.5, the subclass separators converge in the [CaH2+CaH3,TiO5] plane, and the subclass assignment becomes increasingly uncertain given the inevitable uncertainty in the measurement of the spectral indices. The chance of a misclassification therefore becomes significant for stars of earlier subtypes. As it turns out, one finds in the reduced proper motion diagram a significant number of subdwarfs which are well within the normal locus of the M dwarfs. Because the reduced proper motion is correlated with the velocity of a star *in the plane of the sky*, one would expect, statistically, to find a small fraction of halo subdwarfs to have relatively small reduced proper motions, simply because of a small *projected* velocity. In Fig.7 one actually finds a small number of late-type ($V-J>3.5$) M subdwarf to hover significantly above the main halo subdwarf locus, and this can be explained statistically from projection effects. However, the large clustering of early-type M subdwarfs located well above the main subdwarf locus ($H_V<16$) is so clearly distinct that it is unlikely to be explained by projection effects alone. The suspicion for those stars is that many of them have probably been misclassified.

The problem most likely lies in the accuracy of the CaH/TiO bandhead measurements. With the subclass separators converging in the [CaH2+CaH3,TiO5] plane for subdwarfs of earlier subtypes, the metallicity subclass assignment is bound to be increasingly sensitive on the measurement errors. At this time, so it appears, the accuracy of our spectral index measurements is not good enough to unambiguously classify many of the early-type M dwarfs on our list. We therefore caution that a higher signal-to-noise ratio is required to properly classify M dwarfs/subdwarfs of earlier spectral subtype.

4. COMPARISON WITH THE NEXTGEN MODEL GRID

To estimate the range of [Fe/H] actually associated with each of the metallicity subclasses, we examine the range of CaH2, CaH3, and TiO5 spectral indices predicted by the NextGen model atmosphere grid of Hauschildt, Allard, & Baron (1999). Synthetic spectra for cool stars were retrieved from the website of the PHOENIX

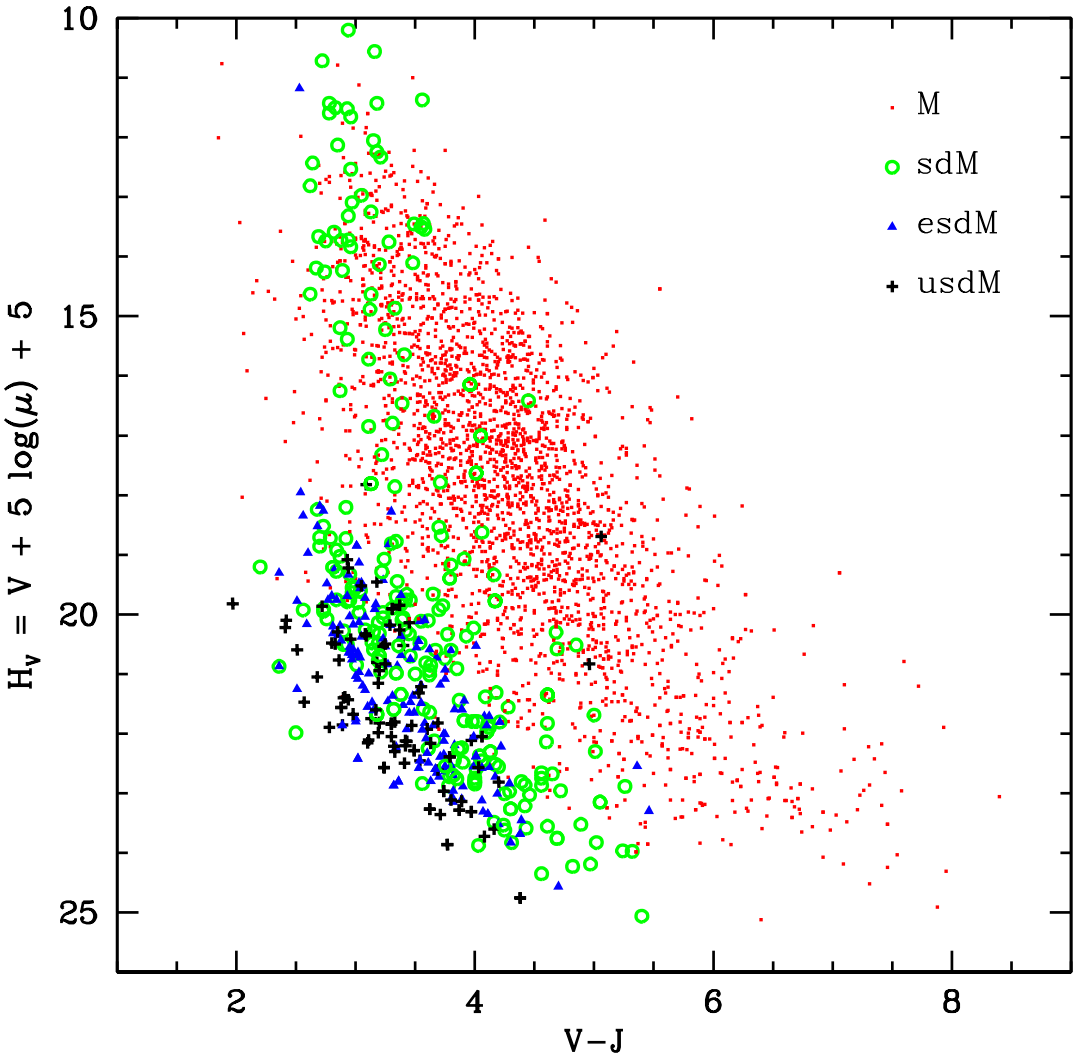

FIG. 7.— Distribution of the spectroscopically confirmed dwarfs and subdwarfs in the (H_V,V-J) reduced proper motion diagram. Dwarfs are plotted as red dots, subdwarfs (sdK,sdM) are plotted as open green circles, extreme subdwarfs (esdK,esdM) as filled blue triangles, and ultra subdwarfs as black crosses. Nearly all subdwarfs fall in the part of the diagram where halo stars are expected to cluster (see Fig.2). There is also a segregation between the sdM/esdM/usdM stars, with the more metal-poor objects having increasingly bluer color and/or larger reduced proper motions. A significant number of stars classified as early-type M subdwarfs ($V-J<3.5$) are located well within the dwarf stars locus, which suggest that at least some of these have been misclassified. This is likely due to the limited range of TiO bandstrengths in the early-type stars, which makes the metallicity subclass assignment more uncertain.

project[5]. We used a grid of spectra with effective temperatures $3,000 < T_eff < 4,000$, $logg$ = 5.0, and metallicities $logZ$ = 0.0,−0.5,−1.0, and −2.0. The high resolution spectra were convolved with a Gaussian kernel to match the appearance of the low-resolution spectra from our spectroscopic follow-up survey. The distribution of CaH2+CaH3 and TiO5 spectroscopic indices are shown in Figure 8.

We find that the NextGen grid points overall provide a theoretical support of only the more general effects of metallicity on the TiO to CaH bandstrength ratio. The model basically confirms that the lower the metallicity, the weaker the TiO bandstrength relative to CaH. However, there are significant discrepancies between the location of the NextGen grid points and our phenomenological definition of the metallicity subclasses. The NextGen model grid clearly does not yield accurate predictions of TiO to CaH ratios. The strongest evidence for this argument is in the locus of the log Z = 0.0 objects (filled circles), which should be expected to fall along the empirically calibrated, mean locus of Galactic disk stars as determined in §3 (dashed line in Fig.8). The source of this discrepancy is that the TiO to CaH ratio tends to be overestimated, in the NextGen grid, for the coolest objects (Burgasser, Cruz, & Kirkpatrick 2007).

Perhaps a cause for more concern is the fact that our subclass separators do not seem to run parallel to the lines of iso-metallicity from the NextGen grid. In particular, our subclass separators have increasing slopes for decreasing values of TiO5, while the NextGen iso-metallicity grid lines show a decreasing slope for decreasing values of TiO5. The discrepancy is most pronounced for CaH2+CaH3<1. It is possible that there is an inflection in the locus of the metal-rich stars due to a saturation of the TiO band, in which case it would be

[5] http://www.hs.uni-hamburg.de/EN/For/ThA/phoenix/

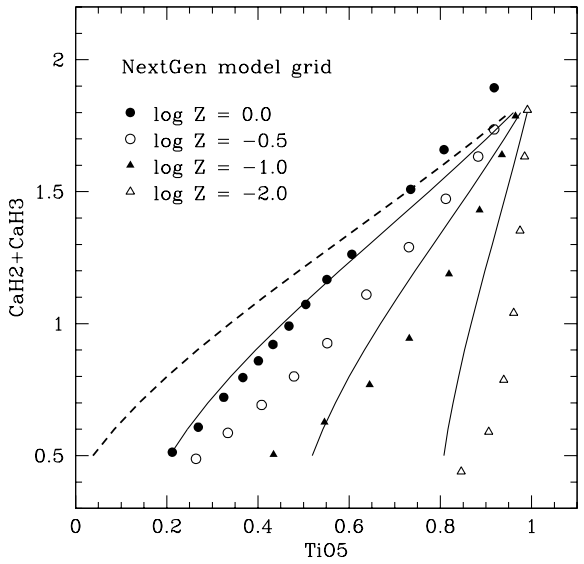

FIG. 8.— Distribution of CaH2+CaH3 and TiO5 indices measured for synthetic spectra from the NextGen model grid (Hauschildt, Allard, & Baron 1999), based on a grid of log g=5.0 models with various T_{eff} and metallicities (see legend). Data points are overlaid on the the new classification grid, with the dashed line showing the observed locus of metal-rich disk stars (log Z=0) and the continuous lines mapping the boundaries between the four metallicity subclasses, as defined in this paper. The disagreement between the NextGen models and our classification scheme is discussed in the text.

inappropriate to carry down this inflection to the metal-poor stars range.

Ultimately, one would want to calibrate the iso-metallicity contours empirically, perhaps using subgroups of chemically homogeneous, metal-poor stars, such as groups of cool subdwarfs from globular clusters. This is unfortunately not possible at this time, for lack of spectroscopic data on cool subdwarfs in clusters. Metallicity segregation of field stars based on kinematical selection appears to be impractical, since all metal-poor stars in our sample at first glance appear to have similar (halo-like) kinematics and cannot be separated into distinct kinematical subgroups.

The best method for properly mapping out the lines of iso-metallicity in the [CaH2+CaH3,TiO5] will probably be to assemble a large sample of resolved subdwarf binaries, and expand on the procedure illustrated in Fig.6. A large area of the diagram (0.2<TiO5<0.7, 0.5<CaH2+CaH3<0.9) remains non-validated at this time. Efforts should be devoted to identifying additional pairs of common proper motion subdwarfs, particularly pairs for which at least one component has CaH2+CaH3<1.0, which would correspond to a spectral subtype later than ≈sdM4.0/esdM4.0/usdM4.0. Accurate measurement of spectral indices in such double stars would be critical in refining the cool subdwarf classification system.

5. DETERMINATION OF SPECTRAL SUBTYPES IN THE COOL SUBDWARFS

The assignment of spectral subtypes for cool subdwarfs and extreme subdwarfs is traditionally based on the depth of the CaH molecular bands. The depth of TiO bands are widely used in the classification of low-mass dwarfs, but TiO bandstrengths show too much dependence on the metallicity to be useful in the subdwarf regime. In the classification system of G97, spectral subtypes of subdwarfs and extreme subdwarfs are determined from the CaH2 and CaH3 indices using these relationships:

$$Sp_{\rm CaH2} = 7.91\ {\rm CaH2}^2 - 20.63\ {\rm CaH2} + 10.71$$
$$Sp_{\rm CaH3}|_{sd} = 13.78 - 16.02\ {\rm CaH3}$$
$$Sp_{\rm CaH3}|_{esd} = 11.50 - 13.47\ {\rm CaH3}$$

Spectral subtypes for the subdwarfs (Sp_{sd}) and for the extreme subdwarfs (Sp_{esd}) are thus formally assigned using slightly different equations:

$$Sp_{sd} = 0.5(Sp_{\rm CaH2} + Sp_{\rm CaH3}|_{sd})$$
$$Sp_{esd} = 0.5(Sp_{\rm CaH2} + Sp_{\rm CaH3}|_{esd}).$$

The reason why separate relationships were used for dwarfs and subdwarfs has to do with the fact that the CaH2 and CaH3 indices are not strictly correlated to each other, and in fact their ratio appears to be a function of metallicity. The $Sp_{\rm CaH2}$ relationship was actually borrowed from the spectral subtype relationship of dwarf stars and, as a result, distinct $Sp_{\rm CaH3}$ relationships had to be defined for the subdwarfs and extreme subdwarfs.

The relationships defined in G97 were based on the original spectroscopic sample of only 79 objects, a sample much smaller than the one currently available. This original sample was particularly deficient in late-type stars, with only two sdM5.0 and one sdM7.0 as the latest subdwarfs, and an esdM5.5 as the latest extreme subdwarf. Cooler object which were discovered afterward, were classified from a simple extrapolation of the relationships above. Figure 9 shows the variation of the CaH2, CaH3, and combined CaH2+CaH3 indices as a function of assigned spectral subtypes. Red continuous lines show the assumed relationship between the indices and the spectral subtypes, in the G97 system.

The assignment of spectral subtypes in the new four-class system introduces a conundrum. Spectral subtyping for the dwarf stars is already very well established, and needs not be changed. But the spectral subtypes for three subdwarf classes is evidently in need of revision, because the original sdM and esdM classes used slightly different relationships and because the new sdM/esdM/usdM subclasses do not have a strict correspondence to the older ones. One solution is to retain the use of $Sp_{\rm CaH2}$ as a fiducial, and redefine new $Sp_{\rm CaH3}$ calibrations for each of the sdM, esdM, and usdM subclasses. However, the reason why CaH2 and CaH3 are not strictly correlated comes from the fact that the CaH2 index is defined in a region of a CaH band which is also overlapped with a major TiO band extending redward from ≈ 6700Å. This is most obvious in the metallicity sequence show in Fig.4, and implies that values of the CaH2 index must be a function of metallicity in the subdwarfs. Hence using a metallicity-dependent index to define the spectral subtypes does not sound like the best choice.

Another solution might be to redefine the spectral subtypes based on the strength of the CaH3 index alone, which is not so obviously dependent on the metallicity. Unfortunately, the CaH3 index doesn't constrain the subtype sequence as well as CaH2 for earlier spectral subtypes. This is clear from Figure 10, which shows the observed relationship between the CaH2 and CaH3 indices. The CaH2 index decreases faster than CaH3 for index values larger than ≈ 0.5. The trend is reversed for late-type stars, because the CaH2 gets close to saturation and slowly becomes degenerate. While it would be tempting to use the CaH2 index in early-type objects and the CaH3 index in late-type objects, this would make spectral

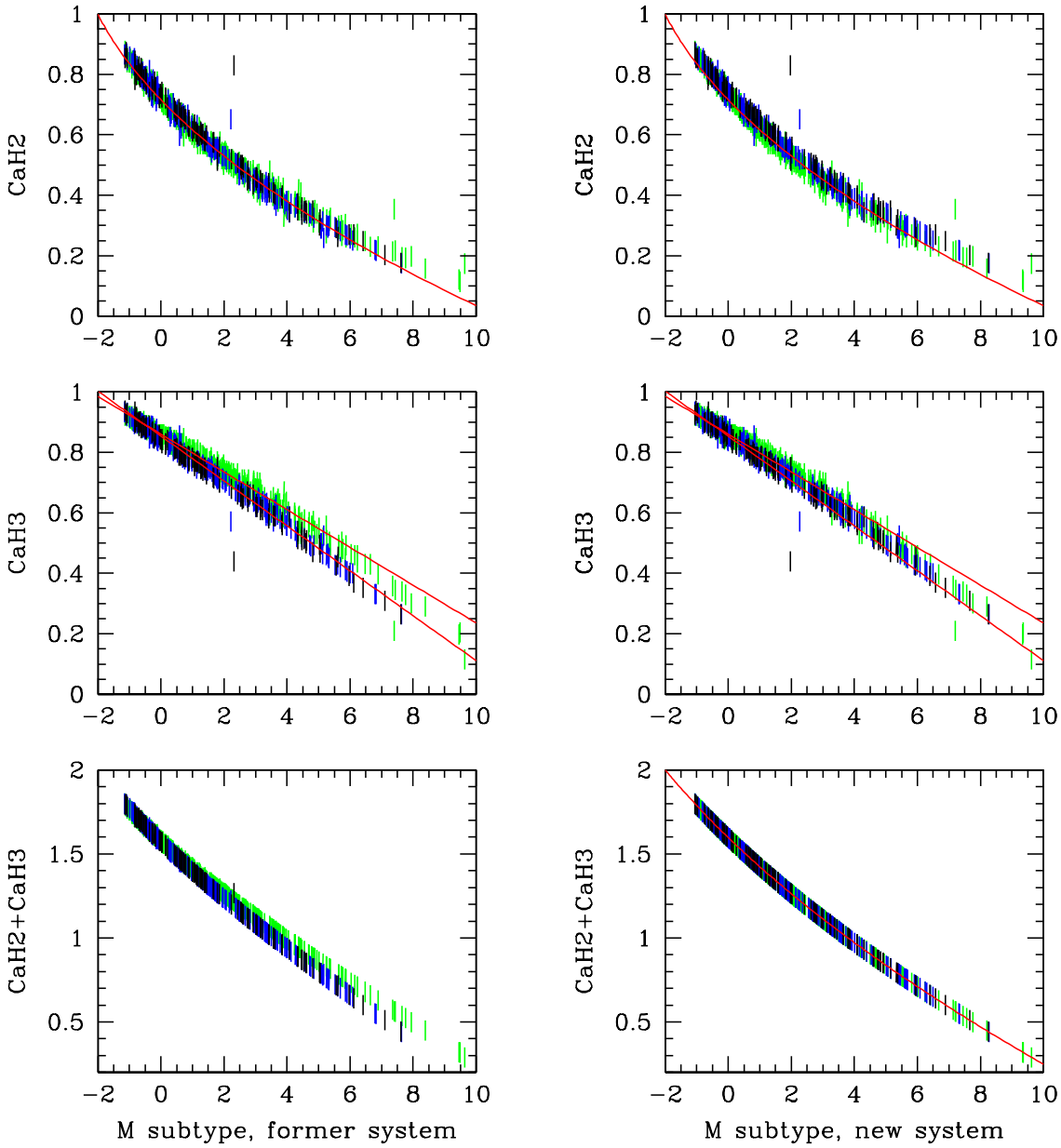

FIG. 9.— Left panels: variation in the CaH spectral indices with spectral subtype, for subtypes assigned in the system of G97. Separate plots are shown for the CaH2 index (top), the CaH3 index (middle), and the combined CaH2+CaH3 index (bottom). For more clarity, subtype values have *not* been rounded up to the nearest half subtype, as would be customary. Subdwarfs are shown in green, extreme subdwarfs in blue, ultra subdwarfs in black. The G97 system assigns subtypes based on the average of a set of relationships using the CaH2 and CaH3 indices, and uses different relationships for subdwarfs and extreme subdwarfs (red curves); note the slight discrepancy for subdwarfs of later subtypes. Right panels: variation in the CaH spectral indices with spectral subtype, for subtypes assigned according to Equation 4 in this paper. Separate plots are shown for the CaH2 index (top), the CaH3 index (middle) and the combined CaH2+CaH3 index, on which Eq.5 is based (bottom). The new relationship for subtype assignment (red curve), simplifies the classification system as the same relationship is used for all subclasses. The most significant results is in the subtype assignment of late esdM/usdM, which are classified 0.5-1.0 subtype later in the new system.

subtype assignment non-straightforward, as it would require pre-assigning a spectral subtype.

Our best compromise is to assign spectral subtypes simply based on the combined value of the CaH2 and CaH3 indices. The use of CaH2+CaH3 also fits well with our metallicity subclass assignment, which is also dependent on CaH2+CaH3. We find that we can use the relationship:

$$Sp = 1.4(\mathrm{CaH2}+\mathrm{CaH3})^2 - 10.0(\mathrm{CaH2}+\mathrm{CaH3}) + 12.4, \quad (3)$$

which yields a spectral subtype assignment which very closely fits the assignment in the G97 system, with only minor differences. We adopt Equation 4 as a general relationship for assigning spectral subtypes for subdwarfs, extreme subdwarfs, and ultra subdwarfs. Panels on the right in Fig.9 show how CaH2 (top), CaH3 (middle), and CaH2+CaH3 (bottom) vary within the new spectral subtype system.

The main difference between the old and new systems occurs at the latest subtypes for extreme subdwarfs, which tend

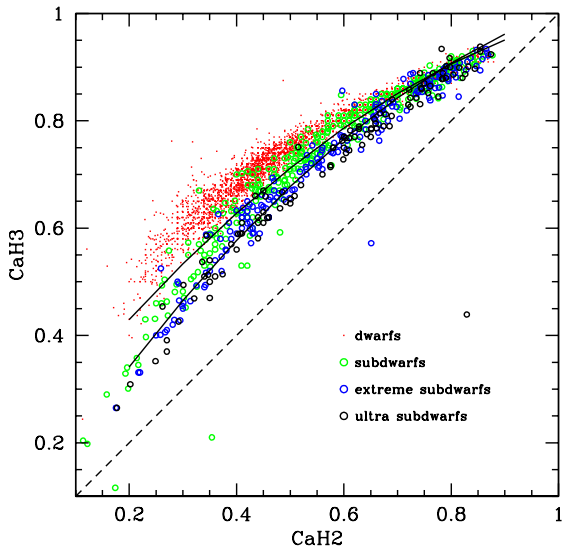

FIG. 10.— Distribution of the CaH2 and CaH3 spectral indices for dwarfs and subdwarfs. Objects are segregated according to their metallicity, with the dwarfs in particular occupying a locus up and to the left of the distribution. The distribution suggests that at least one of the two indices is dependent of metallicity. The likely culprit is CaH2, which probably includes a contribution from a nearby TiO band, and thus presents a deeper band in more metal rich stars.

to be classified with 0.5-1.0 subtypes later in the new system. Hence the star 2MASS 1227-0447, classified as esdM7.5 by Burgasser, Cruz, & Kirkpatrick (2007), is now classified as usdM8.5 in our new system, using the same spectral index values.

6. CLASSIFICATION STANDARDS FOR THE SUBDWARF, EXTREME SUBDWARF, AND ULTRA SUBDWARF SEQUENCES.

We are now assigning metallicity subclasses and spectral subtypes to all the stars observed in our spectroscopic survey using the new four-class system described above. In its current form, the new classification system remains entirely based on values taken by the three spectroscopic indices CaH2, CaH3, and TiO5, as in the former 3-class system of G97.

Traditionally, however, formal spectral classification has often been determined by comparing a target to a set of reference objects formally defined as "classification standards". The use of classification standards makes possible the determination of spectral subtypes using any other part of the spectral energy distribution, by direct comparison with the standards, thus possibly freeing one from the need to always obtain spectra of the same narrow spectral region. This is the essence of the MK process, as elaborated by, e.g., Morgan & Keenan (1973).

From our census of high proper motion subdwarfs, we have assembled sequences of objects to be used as standard sequences for the classification of subdwarfs, extreme subdwarfs, and ultra subdwarfs. These standards were selected based on the following criteria: (1) a spectrum representative of their specific subclass and subtype, (2) a star among the brightest objects of their respective subclass and subtype, (3) an available spectrum with the best possible signal-to-noise ratio, and (4) a location of the sky $-30^\circ <$Decl.$< +30^\circ$ to make the star visible from both hemispheres. We tried to follow those guidelines as much as possible, only skipping stars from the literature for which we could not obtain a copy of the original spectra. A list of the proposed standards is given in Table 2.

Spectra of all standards are displayed in Figure 11. Our standard sequence for subdwarfs (sdM) spans the range from sdK7 to sdM8.0. The sequences for the extreme subdwarfs (esdM) extends to esdM8.5, and the ultra subdwarf (usdM) sequence extends to usdM8.5. A handful of stars of even later subtypes have been reported in the literature (Scholz, Lodieu, & McCaughrean 2004; Burgasser, Cruz, & Kirkpatrick 2007) which could be used to extend the sequence into the L subdwarfs regime. Because of the paucity of such extremely cool stars, we refrain from extending the sequence until more data has been assembled. In any case, it is not obvious that the relationships defined here for the classification of earlier objects should apply to the coolest M dwarfs, and into the L subdwarfs regime. In the ultra-cool dwarfs and subdwarfs, condensate formation depletes Ca and Ti, and the deepening and broadening of the K I absorption doublet obscures the 7000Åregion (Kirkpatrick *et al.* 1999). Other features in the red optical spectra would probably be more useful in extending the scheme to later objects (e.g. Kirkpatrick et al. 1995).

It should also be noted that at the latest subtypes, the CaH index is much more sensitive to variations in metallicity. It has been suggested that for the ultra-cool subdwarfs, a *mild subdwarf* class (denoted d/sd) could be defined (Burgasser, Cruz, & Kirkpatrick 2007); the high proper motion star SSSPM 1444-2019, tentatively classified as d/sdM9, would be the prototype for this intermediate class of objects. The colors of late subdwarfs show a wide distribution which appear to be a function of metallicity (Scholz *et al.* 2004b); color-color scheme might prove useful in further refining or "fine-tuning" the metallicity subclasses for cooler objects.

7. CONCLUSIONS

We have redefined the three metallicity subclasses of low-mass stars of spectral type M based on a recalibration of the TiO to CaH bandstrength ratio, in the spectral region around 7000Å. The new definition retains the dwarf (K5-M9), subdwarf (sdK5-sdM9) and extreme subdwarf (esdK5-esdM9) classes, but introduces a new subclass of objects, the ultra subdwarfs (usdK5-usdM9), which comprise all the stars with the smallest observed apparent metallicity. The different subclasses are redefined based on the ratio of the TiO to CaH bandstrengths, which is correlated with metallicity. The TiO to CaH ratio is calibrated using a subsample of kinematically selected disk stars of presumably solar abundances. A metallicity parameter, $\zeta_{\rm TiO/CaH}$ (see Eq.4), provides a numerical estimate of how the TiO to CaH ratio in a star compares to the value measured in solar-metallicity objects. Stars with close to solar abundances have $\zeta_{\rm TiO/CaH} \simeq 1$, by definition, while metal-poor stars have $\zeta_{\rm TiO/CaH} < 1$, with a value close to 0 representing stars with virtually no detectable TiO molecular absorption, indicative of an ultra-low metal content.

We have also redefined the assignment of the spectral subtypes in all three metallicity sequences based on the sum of the CaH2 and CaH3 indices (CaH2+CaH3). We introduce three sequences of representative objects for each of the three metallicity classes, covering the range of spectral subtypes. These objects should be useful as spectroscopic classification standards. Most standards are located in the northern sky, between declinations 0 and +30. Future efforts should be invested in finding additional standard objects at southern de-

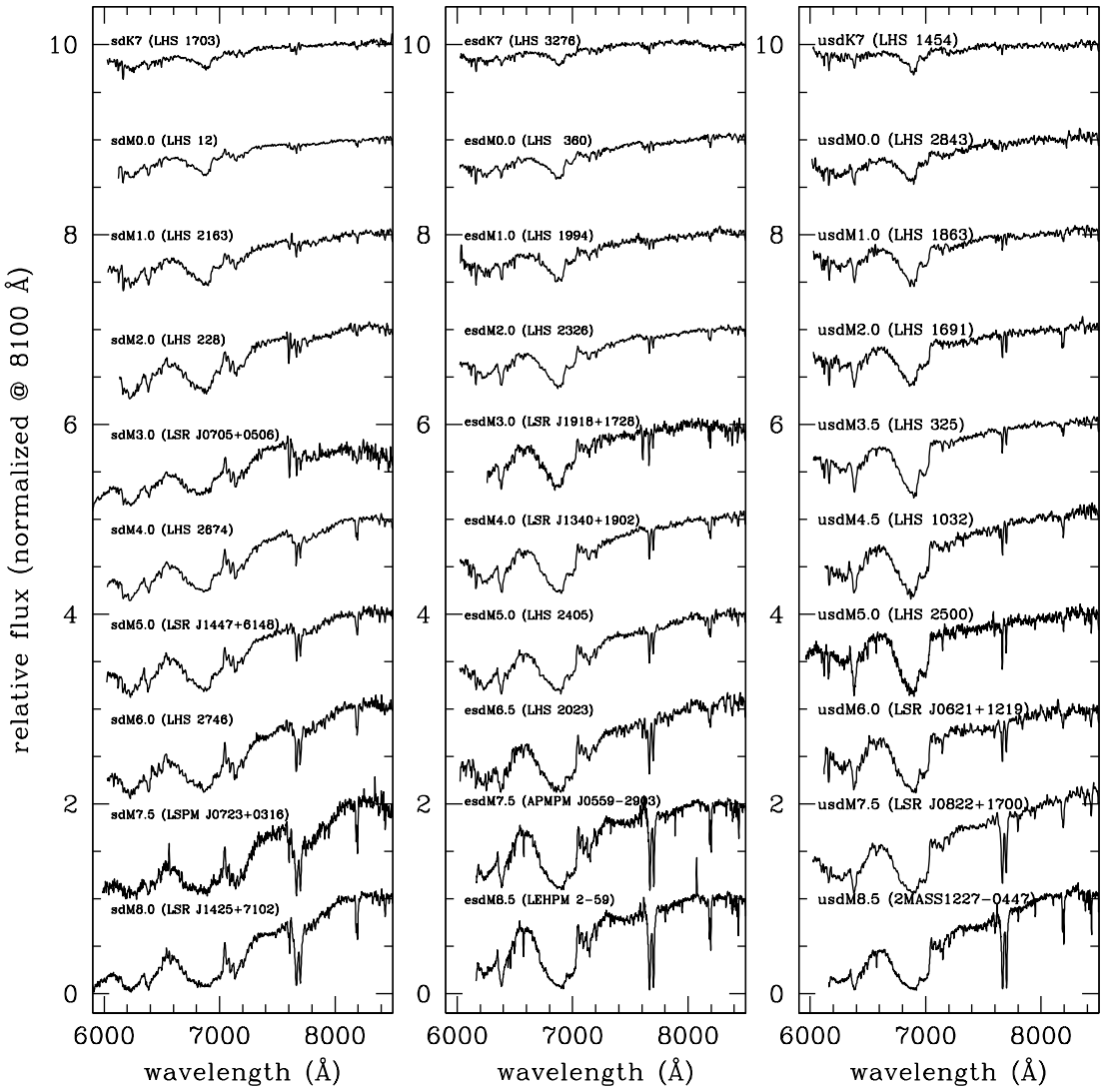

FIG. 11.— Sequences of classification standards for low-mass subdwarfs (left), extreme subdwarfs (center), and ultra subdwarfs (right). Data on those stars are found in Table 2. Metallicity classes (sd, esd, usd) are based on the ratio of the TiO bandhead blueward of 7000Åto the CaH bandhead redward of 7000Å(see §4). All the spectra shown are from our follow-up survey, except spectra from the esdM7.5 star APMPM J0559-2903, the esdM8.5 star LEHPM 2-59, and the usdM8.5 star 2MASS1227-0447, all three graciously provided by A. Burgasser.

clinations.

Ultimately, the use of the TiO/CaH bandstrength ratio as an effective measure of the metallicity in low-mass stars, through the parameter $\zeta_{TiO/CaH}$ should be vetted against independent measurements of the metallicity in selected low-mass, metal-poor stars. Such critical metallicity calibration has now been initiated based on atmospheric modeling of Fe lines using high resolution spectra of bright (mostly early-type) M dwarfs and subdwarfs (Woolf & Wallerstein 2005, 2006; Bean *et al.* 2006). A calibration of the $\zeta_{TiO/CaH}$ parameter with metallicity would be most useful as it would provide a simple means to measure the metallicity in low-mass stars using spectra of only moderate spectral resolution. Abundances could thus potentially be determined for large numbers of distant, faint, low-mass subdwarfs from the Galactic halo, which would become formidable probes of ancient Galactic formation and evolution.

Acknowledgments

The authors would like to thank Adam Burgasser for a critical reading of the manuscript. His comments and suggestions resulted in significant improvements of the paper.

This research program was supported by NSF grant AST-0607757 at the American Museum of Natural History. SL and MS also gratefully acknowledge support from Mr. Hilary Lipsitz.

REFERENCES

Allard, F., & Hauschildt, P. 1995, ApJ, 445, 433
Bean, J. L., *et al.* 2006, ApJ, 652, 1604
Bessel, M. S. 1982, PASAu, 4, 417
Bessel, M. S. 1991, AJ. 101, 662
Burgasser, A., *et al.* 2003, ApJ, 592, 1186
Burgasser, A., *et al.* 2004, AJ, 127, 2856

Burgasser, A., 2004, ApJ, 614, L73
Burgasser, A., & Kirkpatrick, J. D. 2006, ApJ, 645, 1485
Burgasser, A., Cruz, K. L., & Kirkpatrick, J. D. 2007, ApJ, 657, 494
Cushing, M. C., & Vacca, W. D. 2006, AJ, 131, 1797
Cutri, R. M., *et al.* 2003, The 2MASS All-Sky Catalog of Point Sources University of Massachusetts and Infrared Processing and Analysis Center (IPAC/California Institute of Technology)
Gizis, J. E. 1997, AJ, 113, 806 (G97)
Gizis, J. E., & Reid, I. N. 1997, AJ, 113, 806
Gizis, J. E., & Reid, I. N. 1997, PASP, 109, 1233
Gizis, J. E., Scholz, R.-D., Irwin, M., & Jahreiss, H. 1997, MNRAS, 292, L41
Gizis, J. E., Harvin, J. 2006, AJ, 132, 2372
Gould, A. 2003, ApJ, 583, 765
Hartwick, F. D. A., Cowley, A. P., & Mould, J. R. 1984, ApJ, 286, 296
Hauschildt, P. H., Allard, F., Baron, E. 1999, ApJ, 512, 377
Hambly, N. C., *et al.* 2001, MNRAS, 326, 1315
Hawley, S., Gizis, J. E., & Reid, I. N. 1995, AJ, 112, 2799
Jones, E. M. 1971, AJ, 173, 671
Kirkpatrick, J. D., Henry, T. J., & McCarthy, D. W. 1991, ApJS, 77, 417
Kirkpatrick, J. D., Henry, T. J., & Simons, D. A. 1995, AJ, 109, 797
Kirkpatrick, J. D., *et al.* 1999, ApJ, 519, 802
Laughlin, G., Bodenheimer, P., Adams, F. C. 1997, ApJ, 482, 420
Lépine, S., Shara, M. M., & Rich, R. M. 2003a, ApJ, 585, L69
Lépine, S., Rich, R. M., & Shara, M. M. 2003b, AJ, 125, 1598
Lépine, S., Rich, R. M., & Shara, M. M. 2003c, ApJ, 591, L49
Lépine, S., Shara, M. M., & Rich, R. M. 2004, ApJ, 602, L125
Lépine, S., & Shara, M. M. 2005, AJ, 129, 1483
Lépine, S. 2005, AJ, 130, 1680
Lodieu, N., *et al.* 2005 A&A, 440, 1061
Monet, D. G., *et al.* 1992, AJ, 103, 638
Morgan, W. W., & Keenan, P. C. 1973, ARA&A, 11, 29
Phan-Bao, N., & Bessel, M. S. 2006, A&A, 446, 515
Pokorny, R. S., Jones, H. R. A., Hambly, N. C. 2003, A&A, 397, 575
Reid, I. N., Hawley, S., & Gizis, J. E. 1995, AJ, 110, 1838
Reid, I. N., & Gizis, J. E. 2005, PASP, 117, 676
Ruiz, M. T., & Anguita, C. 1993, AJ, 105, 614
Salim, S., & Gould, A. 2002, ApJ, 575, L83
Schweitzer, A., *et al.* 1999, A&A, 350, L62
Scholz, R.-D., Lodieu, N., & McCaughrean, M. J. 2004, A&A. 428, L25
Scholz, R.-D., *et al.* 2004a, A&A, 425, 519
Scholz, R.-D., *et al.* 2004b, A&A, 428, L25
Woolf, V. M., & Wallerstein, G. 2005, MNRAS, 356, 963
Woolf, V. M., & Wallerstein, G. 2006, PASP, 118, 218

TABLE 2
CLASSIFICATION STANDARDS FOR SUBDWARFS (SD), EXTREME SUBDWARFS (ESD), AND ULTRA-SUBDWARF (USD).

Spectral type	LSPM catalog #	other name	R.A. J2000	Decl. J2000	μR.A.[a] $''$ yr^{-1}	μDecl.[a] $''$ yr^{-1}	V[b] mag	V-J[c] mag	CaH2[d]	CaH3[d]	TiO5[d]	$\zeta_{TiO/CaH}$	ref.[e]
Subdwarfs													
sdK7.0	LSPM J0448+2206	LHS 1703	04 48 32.21	+22 06 25.0	0.047	-0.696	14.51	2.92	0.851	0.911	0.952	0.64	L07
sdM0.0	LSPM J0202+0542	LHS 12	02 02 52.15	+05 42 20.5	2.325	-0.714	12.28	2.81	0.749	0.881	0.876	0.60	L07
sdM1.0	LSPM J0828+1709	LHS 2163	09 38 17.53	+22 00 43.6	-0.742	0.015	14.33	3.72	0.631	0.811	0.740	0.76	L07
sdM2.0	LSPM J0716+2342	LHS 228	07 16 27.71	+23 42 10.4	0.940	-0.584	15.48	3.46	0.520	0.742	0.714	0.62	L07
sdM3.0	LSPM J0705+0506	LSR J0705+0506	07 05 48.76	+05 06 17.1	0.185	-0.473	16.42	2.73	0.421	0.680	0.592	0.70	L03b
sdM4.0	LSPM J1303+2328	LHS 2674	13 03 34.84	+23 28 46.3	-0.452	-0.415	16.36	4.68	0.382	0.604	0.554	0.65	L07
sdM5.0	LSPM J0852+1530	LSR J1447+6148	14 48 46.87	+61 48 02.6	0.150	-0.966	19.40	4.56	0.315	0.505	0.452	0.69	L03b
sdM6.0	LSPM J1331+2447	LHS 2746	13 31 28.24	+24 47 10.9	-0.497	-0.225	20.07	4.69	0.305	0.452	0.383	0.75	L07
sdM7.5	LSPM J0723+0316	···	07 23 43.06	+03 16 21.8	-0.102	-0.401	19.80	5.26	0.193	0.329	0.271	0.77	L07
sdM8.0	LSPM J1425+7102	LSR J1425+7102	14 25 05.03	+71 02 09.6	-0.618	-0.170	19.79	5.02	0.198	0.301	0.332	0.73	L03a
Extreme subdwarfs													
esdK7.0	LSPM J1715+3037	LHS 3276	17 15 46.65	+30 37 57.5	-0.175	-0.706	14.66	2.60	0.854	0.894	0.967	0.39	L07
esdM0.0	LSPM J1346+0542	LHS 360	13 46 55.52	+05 42 56.4	-0.766	-0.851	15.43	3.04	0.734	0.850	0.929	0.34	L07
esdM1.0	LSPM J0814+1501	LHS 1994	08 14 33.54	+15 01 07.8	0.293	-0.409	16.63	3.03	0.665	0.793	0.883	0.35	L07
esdM2.0	LSPM J1054+2406	LHS 2326	10 54 25.89	+24 06 44.5	-0.455	-0.490	16.46	3.62	0.553	0.723	0.847	0.32	L07
esdM3.0	LSPM J1918+1728	LSR J1918+1728	19 18 36.99	+17 28 00.2	-0.131	-0.621	19.05	3.81	0.447	0.662	0.837	0.28	L03b
esdM4.0	LSPM J1340+1902	LSR J1340+1902	13 40 40.68	+19 02 23.1	-0.455	-0.803	18.47	5.46	0.381	0.558	0.799	0.28	L03b
esdM5.0	LSPM J0843+0600	LHS 2405	08 43 58.45	+06 00 39.4	0.314	-0.393	18.50	3.74	0.342	0.494	0.758	0.31	L07
esdM6.5	LSPM J0830+3612	LHS 2023	08 30 51.65	+36 12 57.0	0.398	-0.701	18.27	3.36	0.267	0.406	0.708	0.34	L07
esdM7.5	···	APMPM J0559-2903	05 58 58.64	-29 03 27.2	0.370	0.060	19.50	4.61	0.217	0.331	0.604	0.42	B06
esdM8.5	···	LEHPM 2-59	04 52 09.94	-22 45 08.4	0.064	0.746	19.10	3.60	0.175	0.265	0.656	0.35	B06
Ultra subdwarfs													
usdK7.0	LSPM J0251+2442	LHS 1454	02 51 14.69	+24 42 47.1	0.558	-0.296	16.22	2.41	0.844	0.897	0.998	0.02	L07
usdM0.0	LSPM J1401+0738	LHS 2843	14 01 13.75	+07 38 08.8	-0.528	-0.696	16.68	2.91	0.742	0.889	1.003	-0.02	L07
usdM1.0	LSPM J0642+6936	LHS 1863	06 42 05.77	+69 36 46.7	-0.359	-0.382	16.76	3.09	0.651	0.786	1.002	-0.01	L07
usdM2.0	LSPM J0440+1538	LHS 1691	04 40 14.52	+15 38 51.9	0.087	-0.581	18.27	3.97	0.575	0.717	1.019	-0.04	L07
usdM3.5	LSPM J1221+2854	LHS 325	12 21 32.83	+28 54 22.7	-1.019	-0.295	16.99	3.42	0.440	0.581	0.994	0.01	L07
usdM4.5	LSPM J0011+0420	LHS 1032	00 11 00.78	+04 20 25.0	0.152	-0.515	18.40	4.06	0.374	0.514	0.944	0.08	L07
usdM5.0	LSPM J1202+1645	LHS 2500	12 02 32.29	+16 45 35.3	-0.818	-0.188	19.24	3.77	0.321	0.469	0.978	0.03	L07
usdM6.0	LSPM J0621+1219	LSR J0621+1219	06 21 34.48	+12 19 43.7	0.268	-0.441	18.36	3.60	0.292	0.426	0.971	0.03	L03b
usdM7.5	LSPM J0822+1700	LSR J0822+1700	08 22 33.75	+17 00 18.9	0.359	-0.494	19.80	4.08	0.202	0.309	0.887	0.12	L04
usdM8.5	···	2MASS1227-0447	12 27 05.06	-04 47 20.7	-0.459	0.249	19.40	3.91	0.177	0.265	0.825	0.18	B07

[a] Positions at the 2000.0 epoch and in the J2000 equinox.

[b] Optical V magnitudes estimated from combined photographic blue and red magnitudes in the Digitized Sky Survey, see Lépine & Shara (2005).

[c] Infrared J magnitudes from the 2MASS all-sky catalog of point sources (Cutri *et al.* 2003).

[d] Molecular band indices as defined in Reid, Hawley, & Gizis (1995).

[e] Source of the spectroscopy: L03a – Lépine, Shara, & Rich (2003), L03b – Lépine, Rich, & Shara (2003a), L04 – Lépine, Shara, & Rich (2004), B06 – Burgasser & Kirkpatrick (2006), B07 – Burgasser, Cruz, & Kirkpatrick (2007), L07 – Lepine et al. (2007) in preparation.